NASA-CR-197131

FINAL
IN-46-CR
29 CIT
30946
P. 23

FINAL REPORT

High-Spatial-Resolution
Passive Microwave Sounding Systems

` NASA Grant NAG 5-10

covering the period
February 1, 1980- March 14, 1994

Submitted by

D. H. Staelin and P. W. Rosenkranz

November 1, 1994

Massachusetts Institute of Technology
Research Laboratory of Electronics
Cambridge, Massachusetts 02139

N95-15586

Unclas

63/46 0030946

(NASA-CR-197131)
HIGH-SPATIAL-RESOLUTION PASSIVE
MICROWAVE SOUNDING SYSTEMS Final
Report, 1 Feb. 1980 - 14 Mar. 1994
(MIT) 23 p

FINAL REPORT

High-Spatial-Resolution
Passive Microwave Sounding Systems

ABSTRACT

The principal contributions of this combined theoretical and experimental effort were to advance and demonstrate new and more accurate techniques for sounding atmospheric temperature, humidity, and precipitation profiles at millimeter wavelengths, and to improve the scientific basis for such soundings. Some of these techniques are being incorporated in both research and operational systems.

Specific results include: 1) development of the MIT Microwave Temperature Sounder (MTS), a 118-GHz 8-channel imaging spectrometer plus a switched-frequency spectrometer near 53 GHz, for use on the NASA ER-2 high-altitude aircraft, 2) conduct of ER-2 MTS missions in multiple seasons and locations in combination with other instruments, mapping with unprecedented ~2-km lateral resolution atmospheric temperature and precipitation profiles, atmospheric transmittances (at both zenith and nadir), frontal systems, and hurricanes, 3) ground based 118-GHz 3-D spectral images of wavelike structure within clouds passing overhead, 4) development and analysis of approaches to ground- and space-based 5-mm wavelength sounding of the upper stratosphere and mesosphere, which supported the planning of improvements to operational weather satellites, 5) development of improved multi-dimensional and adaptive retrieval methods for atmospheric temperature and humidity profiles, 6) development of combined non-linear and statistical retrieval techniques for 183-GHz humidity profile retrievals, 7) development of non-linear statistical retrieval techniques for precipitation cell-top altitudes, and 8) numerical analyses of the impact of remote sensing data on the accuracy of numerical weather predictions; a 68-km gridded model was used to study the spectral properties of error growth.

TABLE OF CONTENTS

FINAL REPORT

High-Spatial-Resolution
Passive Microwave Sounding Systems

1. INTRODUCTION

This research project had as its primary objective the development of techniques and theory for measurement of the atmosphere by passive microwave instruments at high spatial resolution. These techniques could eventually be applied to satellite systems. A particular motivation for the work was the planned launch of the Advanced Microwave Sounding Unit (AMSU) on NOAA satellites. A major supporting component of the work reported here was the development of an imaging microwave spectrometer system and its operation on the ground and on a NASA high-altitude aircraft. These microwave observations provided data for studies of clouds, precipitation, and temperature, which are reviewed in Section 2. Section 3 describes several related studies of retrieval techniques which were supported either in whole or in part by this grant.

2. MIT MILLIMETER-WAVE TEMPERATURE SOUNDER

A Instrument Description

The Millimeter-wave Temperature Sounder (MTS) is a dual-band 53/118-GHz microwave radiometer system for the measurement of atmospheric temperature and other phenomena affecting transmission in the microwave absorption bands of molecular oxygen. It is an improved version of an earlier fixed-beam 118-GHz sounder built at MIT and operated aboard NASA's Convair 990 (Ali, et al., 1980). Figure 1 is a block diagram of the present system. The instrument is capable of either downward- or upward-viewing operation on the NASA ER-2 high-altitude aircraft, and also ground-based operation. It has a scanhead, installed in the aft cone of the ER-2 wing superpod, which houses the RF components and a video camera. IF amplifiers, synchronous detectors, integrators, power supplies, temperature controllers, video recorder, and a microcomputer are housed in the midsection of the superpod.

One radiometer is an eight-channel scanning spectrometer with its local oscillator centered on the 118.75 GHz oxygen line. It is a double-sideband superheterodyne system. The eight channels are derived from filters in the IF section, with characteristics given in Table 1. Thus each channel has two symmetrically placed passbands on the sides of the line. Figure 2 shows the weighting functions associated with each channel for the nadir view. This

spectrometer has a stationary scalar feedhorn and subreflector with 7.5° beamwidth which view a step-scanning mirror. The mirror directs energy from a sequence of 14 positions, extending over a 95° angular sector below the aircraft, and also from two calibration targets, into the spectrometer. The integration time per spot is 224 ms, yielding ~ 0.5 K radiometric temperature sensitivity per spot. A scan cycle lasts 5.5 seconds.

The second radiometer is a single-channel (ch.0) fixed-beam nadir-viewing double-sideband superheterodyne system. The antenna has a 10° beamwidth. The local oscillator is tunable under computer control from 52 to 54 GHz. A typical mode of operation would time-share between three or four local-oscillator frequencies, covering roughly the same range of altitudes as the 118 GHz weighting functions. Internal loads are used for calibration of this radiometer.

Table 1. MTS channels' passband specifications.
Channel 0:   L.O. frequency tunable, 52-54 GHz
Channel 1-8:   L.O. frequency fixed, 118.75 GHz

Channel	I.F. Center Freq. (MHz)	I.F. Width (MHz)
0	115	170
1	660	170
2	840	210
3	1040	240
4	1260	220
5	1470	240
6	1670	220
7	1900	270
8	500	125

B   ER-2 Experiments

During the period covered by this grant we participated with the MTS in several NASA experiments involving the ER-2 high-altitude research aircraft. These are listed in Table 2. MTS measurements and retrieved parameters from these experiments have been described by Gasiewski (1988), Gasiewski and Staelin (1989, 1990), Gasiewski, et al.. (1990), Bonnani (1991), and Schwartz et al., (1994a, b). The major results of these papers are summarized below.

Figure 3 shows MTS measurements in a flight track over a series of convective cells during COHMEX. The inset in this figure is an expanded scale showing small perturbations in the two most transparent channels over the visibly opaque cirrus anvil, extending from points A to B, of the rain cell which peaked at C. The cirrus anvil top was at 13-km altitude. The region to the left

of A was visibly clear. These results indicate that the 118-GHz line could be used to infer temperature profiles through thick cirrus clouds, but not through rain. Theoretical calculations of radiative transfer in precipitation cell models (Gasiewski and Staelin, 1990) showed that both liquid and ice phases play significant roles in reproducing measured spectra such as those in Figure 3.

Table 2. Aircraft Experiments

GALE	February, 1986
COHMEX	June-July, 1986
CAPE	July-August, 1991
STORMFEST	February-March, 1992
SSMT-2 Underflights	(West Coast) May;
	(East Coast) July-August, 1992
TOGA-COARE-test flights	January-February, 1993
CAMEX	September-October, 1993

Two hurricanes were overflown with the ER-2: Bob in the North Atlantic in August, 1991, and Oliver in the Coral Sea in February, 1993. Figure 4 displays MTS images of Oliver, as deviations from clear-air brightness temperatures outside the storm (Schwartz, et al., 1994b). These images show a strong response, in the lower-atmosphere channels, to the precipitation in the eyewall and also show smaller cold perturbations from nearby rainbands. At equal pressure levels the clear air inside the eye is warmer than outside. The ~10-K magnitude of the warming over a region of ~50-km diameter in channels 8 and 1 (which are not affected by precipitation) implies that the AMSU-A sounder on future NOAA satellites will be able to monitor the strength of ordinary hurricanes similar to Oliver.

Methods for detection of buoyancy waves in the MTS data were studied by Bonanni (1991). After screening out interference, 14 wavelike events were identified in the GALE and COHMEX datasets, but the largest peak-to-peak amplitude was 0.17 K.

Downlooking measurements with MTS seemed to imply more absorption around 118 GHz than predicted (Gaswieski, 1988). To test this hypothesis, the ER-2 superpod was modified to allow our instrument to be mounted looking upward, and several flights were made this way in 1991-93. This configuration has greater sensitivity to changes in atmospheric opacity. The data is still being analysed, but preliminary results (Schwartz, et al., 1994a) do indicate greater atmospheric opacity at altitudes of 10-20 km. The implications of this, in terms of adjustments to line parameters, is a subject of continuing investigation.

C. Ground-based Measurements

The MTS was operated on the ground at Fryeburg, ME in January 1987, observing zenith. This location is ~38-km southeast of Mt. Washington. Repeated occurances of periodic disturbances in 118-GHz brightness temperature were observed (Bonanni, 1991) during visually opaque conditions at the onset of snowfall. These disturbances were determined to be the effect of modulation of atmospheric opacity due to either water vapor or liquid water (wet snow). The evidence may favor the latter because the fractional changes required in water vapor (~30 percent) are larger than those required in liquid water (~0.007 gm^{-3} in 6-km layer).

D. Upper Stratosphere Sounding Possibilities

Upper-atmospheric emission from the strong oxygen lines cannot be observed either from the surface or from aircraft because the lower atmosphere is opaque. However, on the wings of the 60 GHz band (e.g. 52 to 54 GHz), the opacity of the lower atmosphere is small enough to permit observation of stratospheric emission from lines arising in higher rotational levels (Waters, 1973). Within a few MHz of the line centers, thermal emission from oxygen microwave lines has (in general) partial elliptical polarization, becoming circular for observation along a field line and linear for transverse observations. The polarized component originates at altitudes above 40 km, where line widths are comparable to or less than the Zeeman splitting (Rosenkranz and Staelin, 1988).

At any frequency, most of the brightness temperature is emitted from the lower atmosphere. Therefore, one takes the difference of two measurements, either at different frequencies or different polarizations, to measure the high-altitude emission. The vertical distribution of contributions to this brightness-temperature difference is a contribution function. To obtain a reasonable signal-to-noise ratio, one averages over a finite bandwidth, and thus one may generalize the differencing operation to integration over frequency with antisymmetric weighting. Figure 5 displays a normalized contribution function for left-circular-polarized observations of the 27- line, using a 3.82-MHz wide spectrum weighting function centered at -0.5 MHz from the line center (Rosenkranz, 1990). With a receiver noise temperature of 1300 K, it would be possible to obtain sensitivity to stratopause region temperature of 1 K rms in 20 minutes observation at the surface.

In preparation for future observations of this line, we built a 32-channel autocorrelator board for the computer, using VLSI 2-bit autocorrelator chips (Petro, 1989). Figure 6 is a block diagram of a spectral-line system design.

3. RETRIEVAL THEORY AND ATMOSPHERIC STRUCTURE

A. Water-vapor Profiles

A method for retrieval of water vapor profiles from measurements in the vicinity of the 183-GHz line was developed (Komichak, 1982; Rosenkranz, et al., 1982). The basis of this method is interpolation of two temperature profiles, as shown in Fig. 7. The profile of temperature as a function of water vapor burden (defined as vertically integrated column density overhead) is obtained by linear-least-square estimation using radiometer channels at 90-183 GHz, and the profile of temperature as a function of pressure is obtained from channels at 50-60 GHz. The result of the interpolation is a profile of water vapor burden as a function of pressure. Although this profile could be regarded as an end product, it was used as input to a linear-least-square estimator of relative humidity.

Water vapor profiling was subsequently developed further in papers by Kuo, et al., (1994) and Cabrera-Mercador and Staelin (1994), with support from other grants.

B. Two-and Three-Dimensional Filtering

This work applied the principles of multi-dimensional spatial Wiener filters to the geophysical retrieval problem. The implementation of these filters was done by a fast Fourier transform of radiometric measurements in the spatial domain, followed by linear-least-square estimation of geophysical parameters at each spatial frequency, followed by inverse Fourier transformation.

Applied to Scanning Multichannel Microwave Radiometer data, this approach provided a rigorous treatment of the problem of different antenna beam widths at different frequencies (Rosenkranz, 1982). In this case the filter had two spatial dimensions and one dimension of channel number, which maps into geophysical parameters. The retrieved parameters were sea surface temperature, near-surface wind speed, integrated water vapor, integrated liquid water, and characteristic drop radius.

Applied to Microwave Sounder Unit (MSU) measurements by Nathan, et al., (1985), a two-dimensional spatial filter gave as much as 25% lower temperature profile errors than the conventional one-dimensional least-square estimator. Here the first dimension is altitude (or channel number) and the second dimension is distance along the orbital track. In this problem, the conventional estimator can use only the vertical correlation of atmospheric temperature, whereas the spatial filter had the advantage also of using horizontal correlation.

C. Atmospheric Structure and Estimation of Temperature Fields

Toldalagi (1980) showed how time-varying Markovian models could be derived from atmospheric general circulation models, and then be used to adapt Kalman filters for temperature profile retrievals. The resulting improvements were too modest relative to fixed global Kalman filters to warrant their complexity.

Related attempts to improve temperature profile retrieval performance using tropopause height as input to a linear retrieval (Komichak, 1980) were also insufficiently rewarding; non-linear retrieval techniques might utilize such information more efficiently. Greater improvements (~5-50%) were obtained by Bauman (1980), who used linear retrievals updated by recent geographical relevant observations of measurement means and covariances.

Briancon (1986) further extended the theory of multidimensional retrievals by developing a model for the three-dimensional covariance of temperature, and using it to predict the performance of estimation operators whose supporting domain was finite, infinite, or semi-infinite (Kalman filters). The use of horizontal correlations in various estimation schemes produced typically 15 to 25 percent reduction of rms errors for MSU, and 5 to 10 percent reduction for AMSU (in simulations). Adaptive retrieval operators for nonstationary processes were also considered, and criteria for optimizing these operators were found.

D. Impact of High Spatial Resolution Data on Numerical Weather Prediction

The University of Wisconsin primitive-equation forecasting model was used to study the growth of errors as a function of time and resolution of the data assimilated into the model. The method was to measure the response of the model as a function of wavenumber, by adding geostrophically-balanced perturbations of temperature and wind at various three-dimensional spatial frequencies to the initial fields, and subtracting a control with no perturbations from the perturbed forecasts. Figure 8 shows predicted temperature error energy, summed over 10 levels, as a function of forecast time, with the temperature measurement resolution K_0 as a parameter. At wavenumbers $\geq K_0$ the initial errors are equal to the energy spectrum of the atmosphere, while for wavenumbers $< K_0$, the initial errors result from aliasing. As forecast time increases, errors at all frequencies approach the atmospheric variance due partly to chaotic turbulence processes. Note that from the Nyquist criterion, the distance between measurements is $0.5 \times 10^6 m/K_0$.

Using these results, a new statistical model for error evolution in numerical prediction models was formulated to approximate our observations of error behavior in a University of Wisconsin (Madison) adaptation of a primitive-equations model with limited area, nesting, and semi-implicit time differencing with ten sigma levels (0.09-0.99); grids of 135.2 and 67.6 km were used for the continental U.S. The deduced limit on predictability D (days) is:

$$D < (\lambda_{max}/300)(1 - 2^{[1-\lambda_{max}/\lambda_{min}]})$$

where distances are in kilometers and the equation was deduced from experiments with λ between 135 and 1090 km. The equation assumes we have perfect

knowlege at time zero for wavelengths longer than λ_{max} and zero knowledge otherwise, corresponding to a mean-square difference E between the known temperature field and truth, and that at t = 0+ we learn the true atmosphere for wavelengths longer than λ_{min}, thus reducing E to E'. The limit D is the number of days for which a perfect prediction model could yield an expected mean-square error E" for the predictions which is less than E. Choice of λ_{max} specifies the scale sizes of interest to us in the predictions, and the choice of λ_{min} specifies the spatial resolution of the initialization data for the numerical prediction model. Use of this equation for synoptic scale predictions (λ_{max} = 3000 km) suggests that AMSU resolutions of 100 km will not much improve D(~10 days) over RAOB-based forcasts with λ_{min} =600 km resolution, whereas for mesoscale forcasts with λ_{max} = 1200 km the indicated values of D drop from 4 days for 600-km RAOBs to 2 days with AMSU resolution (100 km).

E. Retrieval of Precipitation Cell-top Altitude

MTS brightness temperature perturbations (cell-center T_B minus clear-air T_B), obtained over precipitation cells such as those shown in Figure 3 were used to develop a technique to infer cell-top altitudes. The algorithm, described by Gasiewski and Staelin (1989), consists of a Karhunen-Loeve transformation and rank reduction of the T_B perturbations, followed by a nonlinear operation and then a linear least-square regression of the transformed variables against the visible cell top altitude, which was measured by stereoscopy using the simultaneous video imagery.

Figure 9 shows the accuracy of the retrieval on an ensemble of 279 independent spectra from GALE and COHMEX. The rms discrepancy between retrieved and visible altitudes is 1.97 Km. Part of this scatter is due to an uncertainty of ~1 km in the optical cell-top altitude. Additional work on the accuracy of cloud height estimates using video stereoscopy from the NASA aircraft was performed by Bayer (1988).

Subsequent work, funded by another grant, on retrieval of cell-top altitudes with a neural network has yielded improved results (Spina, 1994: Spina, et al., 1994). Earlier work by Jin (1981) focused on cloud measurements using Tiros-N MSU data, including the 53.75-GHz channel.

PUBLICATIONS AND THESES SUPPORTED BY THIS GRANT

Baumann, W. T., "Linear Statistical Retrieval as Applied to Remote Sensing of Atmospheric Temperature Profiles," SM thesis, MIT, May (1980).

Komichak, M. J., "Relevance of Tropopause Location to Remote Sensing of Atmospheric Temperature Profiles," SB thesis, MIT, May (1980).

Toldalagi, P. M., "Adaptive Filtering Methods Applied to Satellite Remote-Sensing of the Atmosphere for Meteorological Purposes," Ph.D. thesis, MIT, May, (1980).

Jin, J.-S., "Cloud Detection Using Tiros-N Satellite Data," SM thesis, July (1981).

Staelin, D. H., "Passive Microwave Techniques for Geophysical Sensing of the Earth from Satellites," *IEEE Trans. Antennas Propagat.*, **AP-29**(4), 683-687 (1981).

Rosenkranz, P. W., "Inversion of Data from Diffraction-limited Multiwavelength Remote Sensors 2. Nonlinear Dependence of Observables on the Geophysical Parameters," *Radio Sci.*, **17**(1), 245-256 (1982).

Rosenkranz, P. W., Komichak, M. J., Staelin, D. H., "A Method for Estimation of Atmospheric Water Vapor Profiles by Microwave Radiometry," *J. Appl. Meteor.*, **21**(9), 1364-1370 (1982).

Komichak, M. J., "Estimation of Atmospheric Water Vapor Profiles Using Microwave Radiometry," M.S. thesis, MIT, June (1982).

Nathan, K. S., "Application of a Multi-Dimensional Spatial Filter to Temperature Profile Retrieval," M.S. thesis, MIT, May (1983).

Staelin, D. H., "Atmospheric Temperature Sounding from Space," in <u>Preprint Volume of Extended Abstracts: Ninth Conference on Aerospace and Aeronautical Meteorology June 6-9, 1983,</u> Omaha, Nebr., (published by the American Meteorological Society, Boston, Mass.).

Staelin, D. H., "Passive Microwave Remote Sensing of the Atmosphere from Satellites," in <u>Proceedings of IGARSS'84 Symposium, Strasbourg 27-30 August 1984</u>. Ref. ESA SP-215 (published by ESA Scientific & Technical Publications Branch in August, 1984).

Nathan, K. S., Rosenkranz, P. W., Staelin, D. H., "Temperature Profile Retrieval by Two-Dimensional Filtering," *J. Climate Appl. Meteor.*, **24**(6), 517-524 (1985).

Briancon, A. C. L., "Estimation and Modeling of Multidimensional Non-Stationary Stochastic Processes: Application to the Remote Sensing of Atmospheric

Temperature Fields," Ph.D. thesis, MIT, August (1986).

Bayer, W.R., "Height Estimation of Clouds from Aerial Photography," SB thesis, May (1988).

Gasiewski, A. J., and Staelin, D. H., "Hydrometeor Scattering in 53- and 118-GHz Observations of Brightness Temperatures over Precipitation Cells," in <u>Proceedings 1988 URSI Radio Science Meeting, June 6-10, 1988</u>, pp. 80-84.

Gasiewski, A. J. T., "Atmospheric Temperature Sounding and Precipitation Cell Parameter Estimation Using Passive 118-GHz O_2 Observations," Ph.D. thesis, MIT, December (1988).

Petro, M. C., "An Autocorrelator for Determining the Temperature of the Upper Atmosphere," S.B. thesis, MIT, June (1989).

Gasiewski, A. J. and Staelin, D. H., "Statistical Retrieval of Precipitation Cell-Top Altitude Using Passive 118-GHz Observations," <u>Proc. of IGARSS Conf., Vancouver, B.C. (1989)</u>.

Staelin, D. H., "Passive Microwave Sensing of the Atmosphere from Space," <u>Microwave Radiomet. Remote Sens. Appl.</u> (P. Pampaloni, ed.), 151-167 (1989) VSP.

Gasiewski, A. J., and Staelin, D. H., "Statistical Precipitation Cell Parameter Estimation Using Passive 118-GHz O_2 Observations," *J. Geophys. Res.*, **94**, 18,367-18,378 (1989).

Gasiewski, A. J., Staelin, D. H., "Numerical Modeling of Passive Microwave O_2 Observations over Precipitation," *Radio Sci.* ,**25**(3), 217-235 (1990).

Gasiewski, A. J., Barrett, J. W., Bonanni, P. G. and Staelin, D. H., "Aircraft-based Radiometric Imaging of Tropospheric Temperature and Precipitation Using the 118.75-GHz Oxygen Resonance," *J. Appl. Met.*, **29**, 620-632 (1990).

Rosenkranz, P. W., "Oxygen Line Emission as a Measure of Temperature in the Upper Stratosphere," <u>Proc. of IGARSS Conf., Washington, DC, May 20-24, 1990</u>, pp. 1185-1188.

Bonanni, P. G., "Atmospheric Wave Detection and Parameter Estimation using Passive Measurements of Thermal Emission near 118 GHz," Ph.D. thesis, MIT, February (1991).

Chiarchiaro, W. J., "54-GHz Radiometer for Profiling the Temperature of the Atmosphere," M.S. thesis, MIT, May (1991).

Schwartz, M. J., Barrett, J. W., Rosenkranz, P. W., Staelin, D. H., "Atmospheric Transmittance Measurement Near 54 and 118 GHz," Proc. of IGARSS Conf., Pasadena, CA, Aug. 8-12, 1994a,

Schwartz, M. J., Barrett, J. W., Fieguth, P. W., Rosenkranz, P. W., Spina, M. S., Staelin, D. H., "Passive Microwave Imagery of a Tropical Storm near 118 GHz Thermal and Precipitation Structure," Proc. of IGARSS Conf., Pasadena, CA, Aug. 8-12, 1994b,

Spina, M. S., "Application of Multilayer Feedforward Neural Networks to Precipitation Cell-Top Altitude Estimation," MS thesis, MIT, Sept. (1994).

Other References

Waters, J. W., "Ground-based Measurement of Millimeter-wavelength Emission by Upper Stratospheric O_2, Nature, **242**, 506-508 (1973).

Ali, A. D. S., Rosenkranz, P. W., Staelin, D. H., "Atmospheric Sounding Near 118 GHz," J. Appl. Met., **19**(10) 1234-1238 (1980).

Rosenkranz, P. W., and Staelin, D. H., "Polarized Thermal Microwave Emission from Oxygen in the Mesosphere," Radio Science, **23**(5), 721-729 (1988).

Cabrera-Mercader, C. R., and Staelin, D. H., "Passive Microwave Relative Humidity Retrievals using Feedforward Neural Networks," submitted to IEEE Trans. on Geo. and Remote Sensing. (1994).

Kuo, C. C., Staelin, D. H., Rosenkranz, P. W., "Statistical Iterative Scheme for Estimating Atmospheric Relative Humidity Profiles," IEEE Trans. on Geo. and Remote Sensing, **32**(2), 254-260 (1994).

Spina, M. S., Schwartz, M. J., Staelin, D. H., Gasiewski, A. J., "Application of Multilayer Feedforward Neural Networks to Precipitation Cell-Top Altitude Estimation," Proc. of IGARSS Conf., Pasadena, CA, Aug. 8-12, 1994.
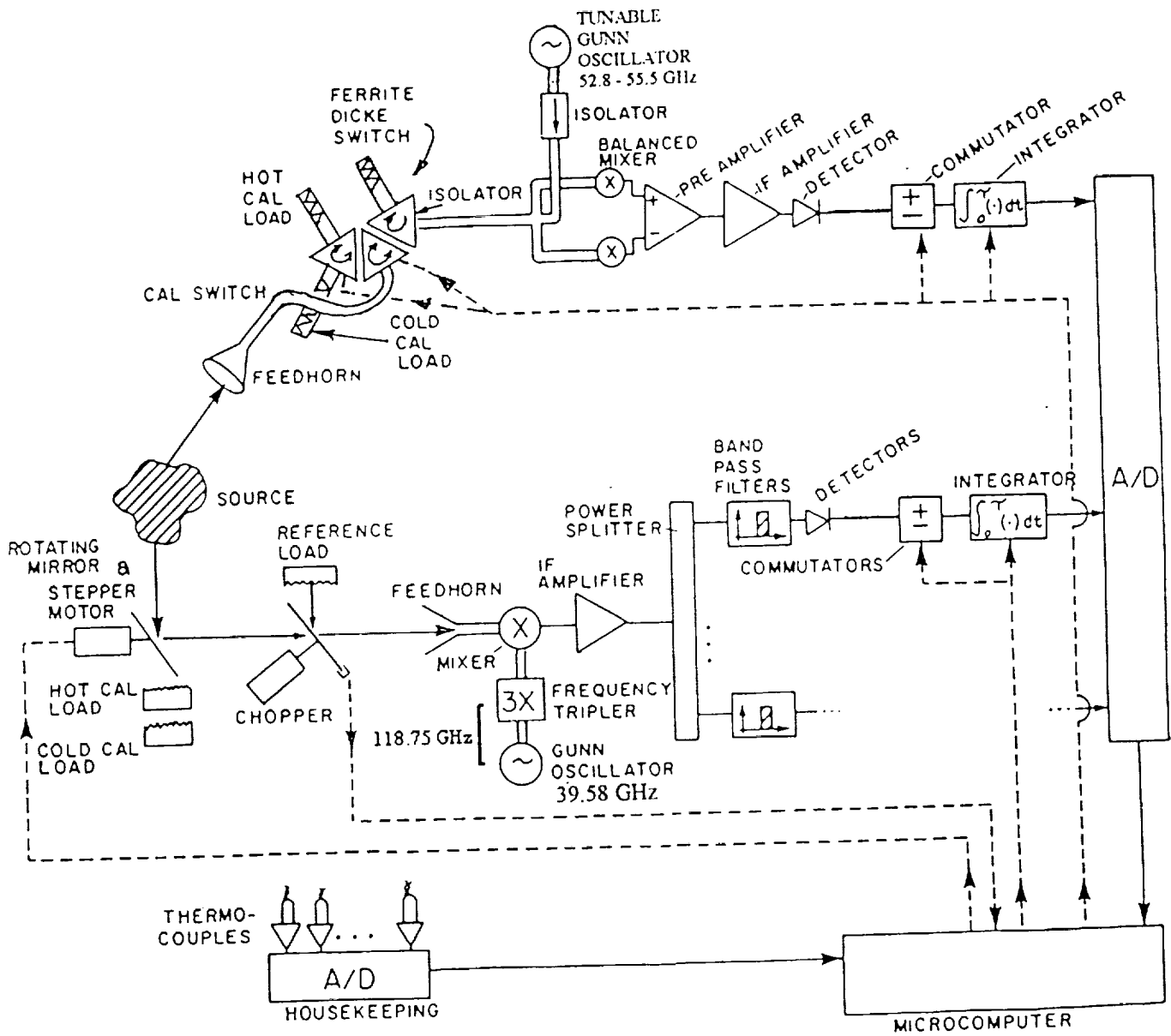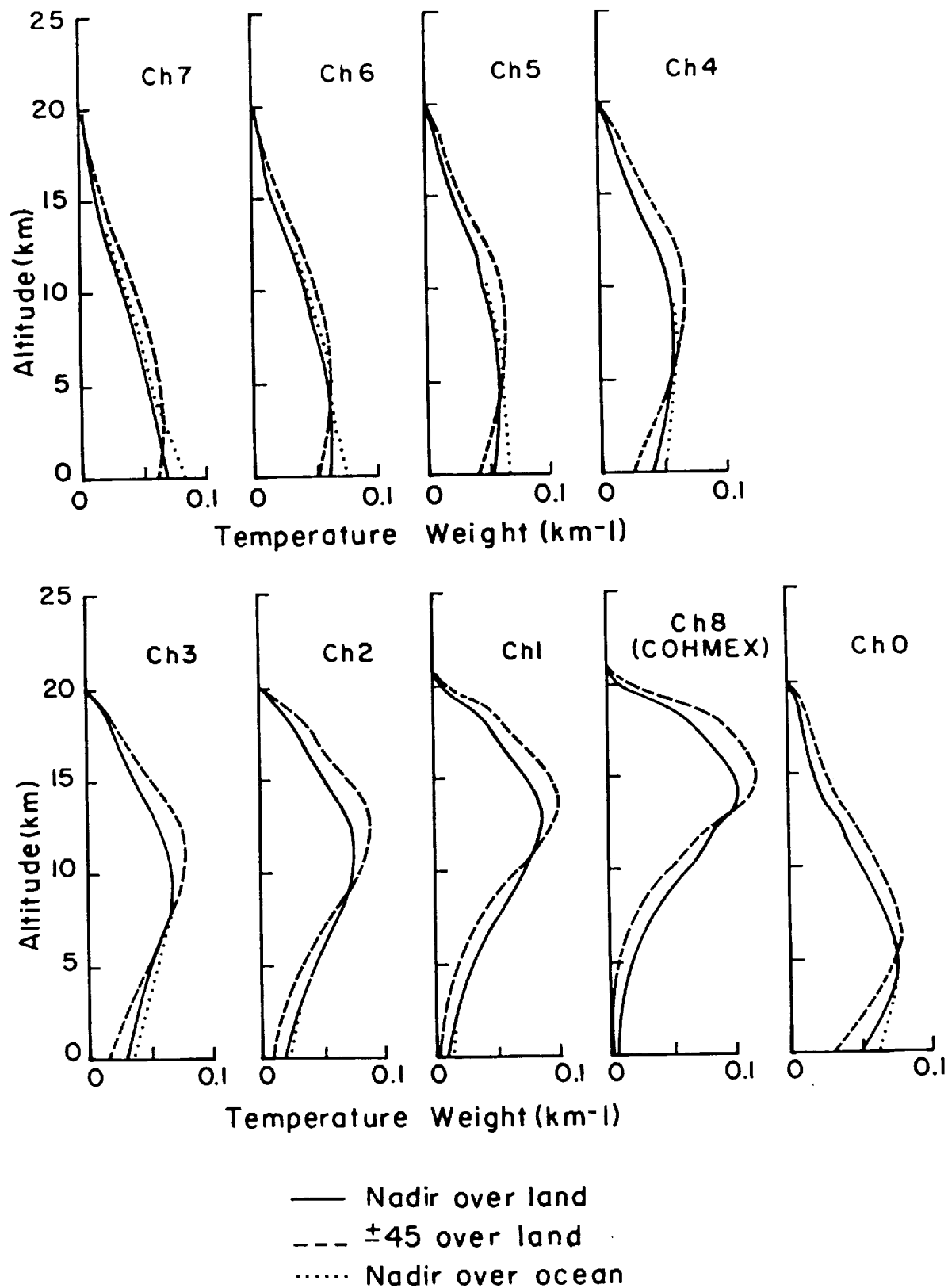
Figure 1. MTS instrument block diagram.

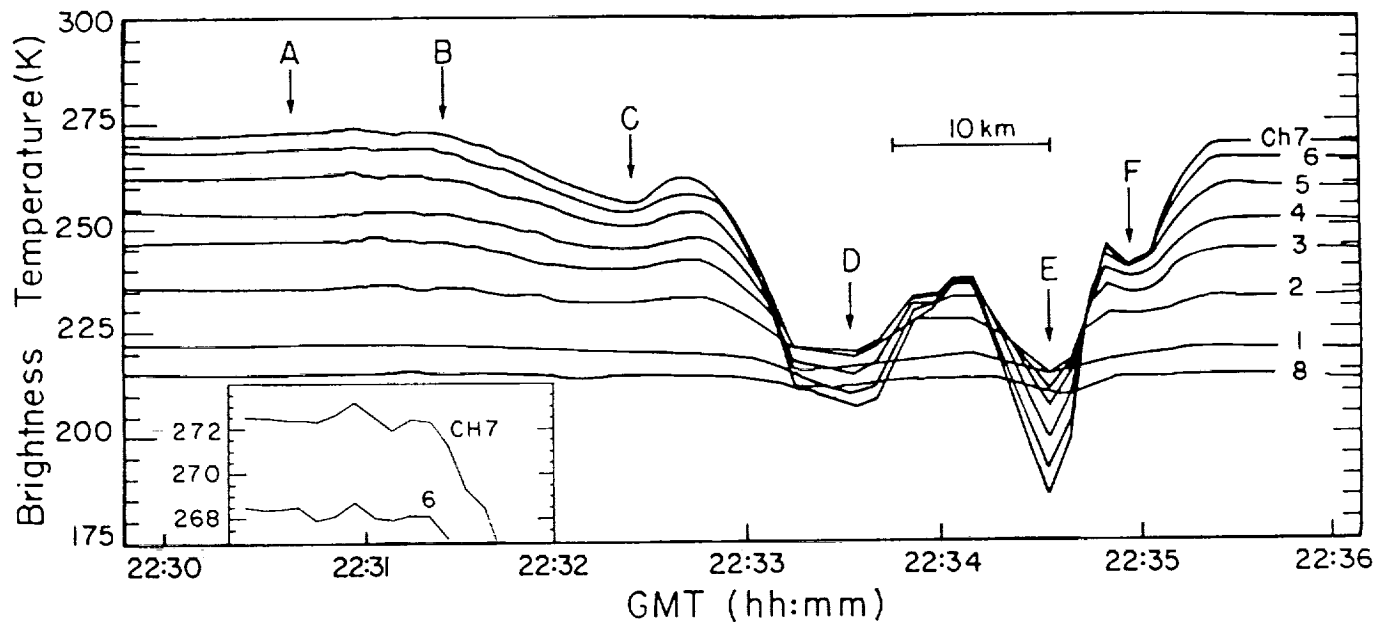Figure 2. MTS weighting functions near 118 GHz.

Figure 3. Brightness temperatures observed near nadir by MTS on July 8, 1986, on a track over a series of convective cells (Gasiewski et al., 1990).
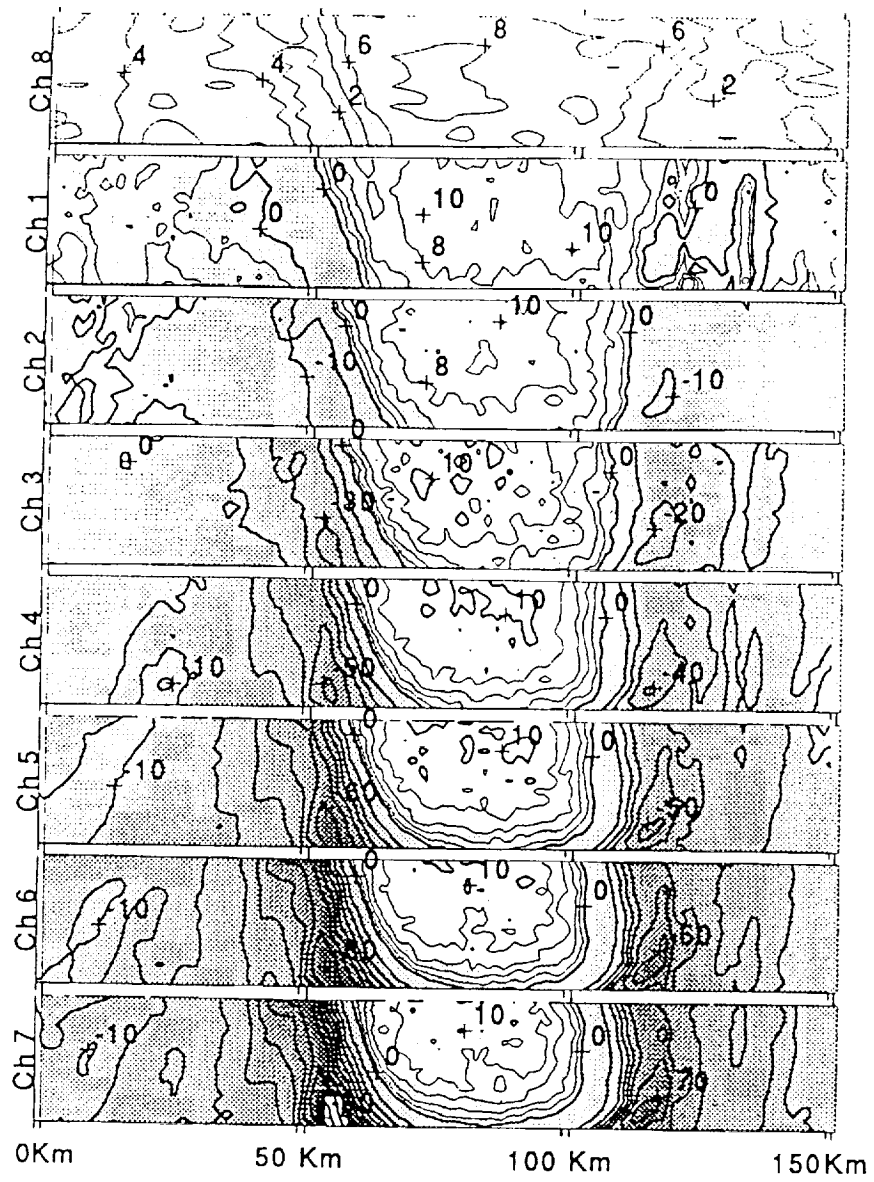
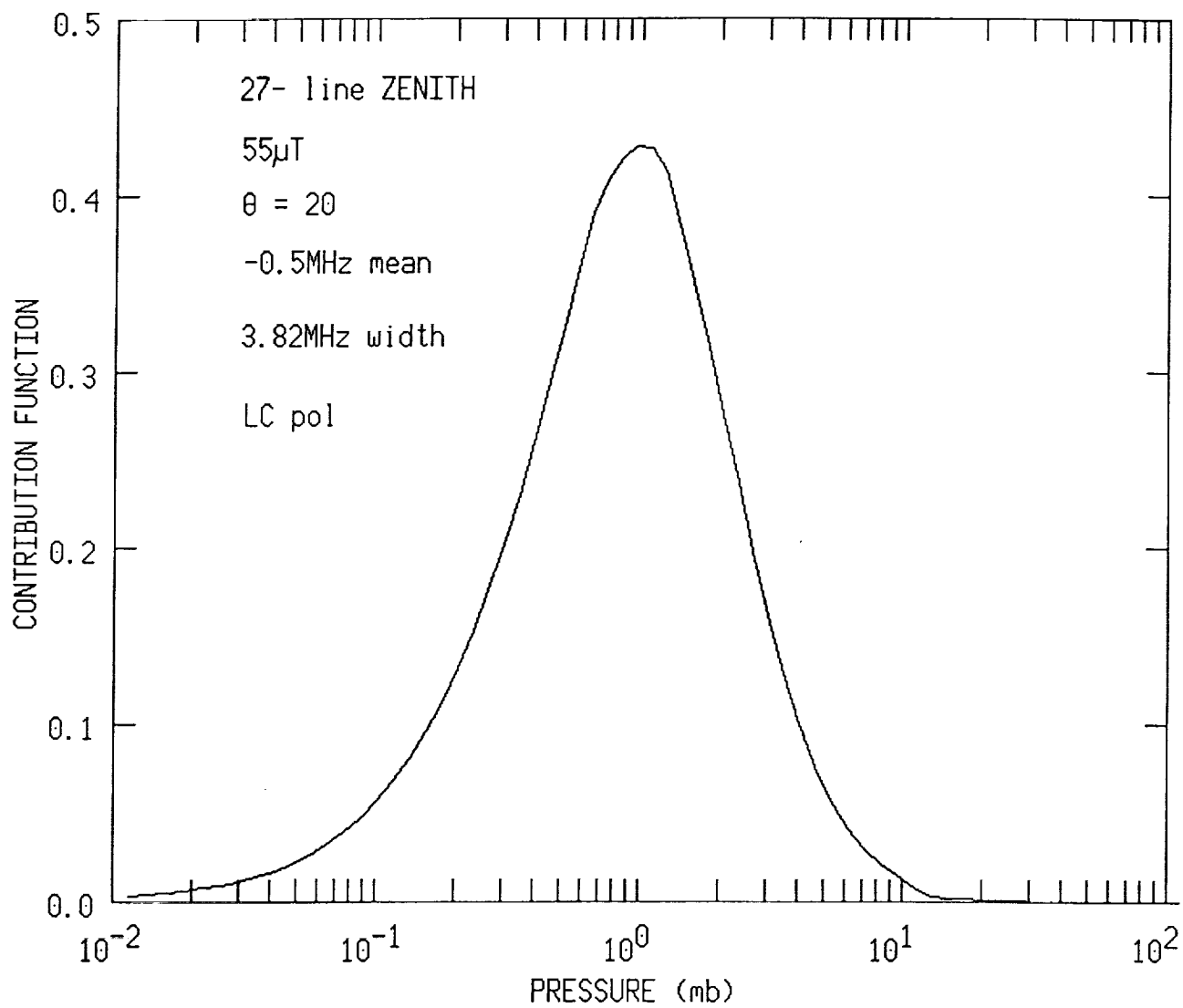Figure 4. MTS brightness temperature perturbations (K) over Cyclone Oliver.

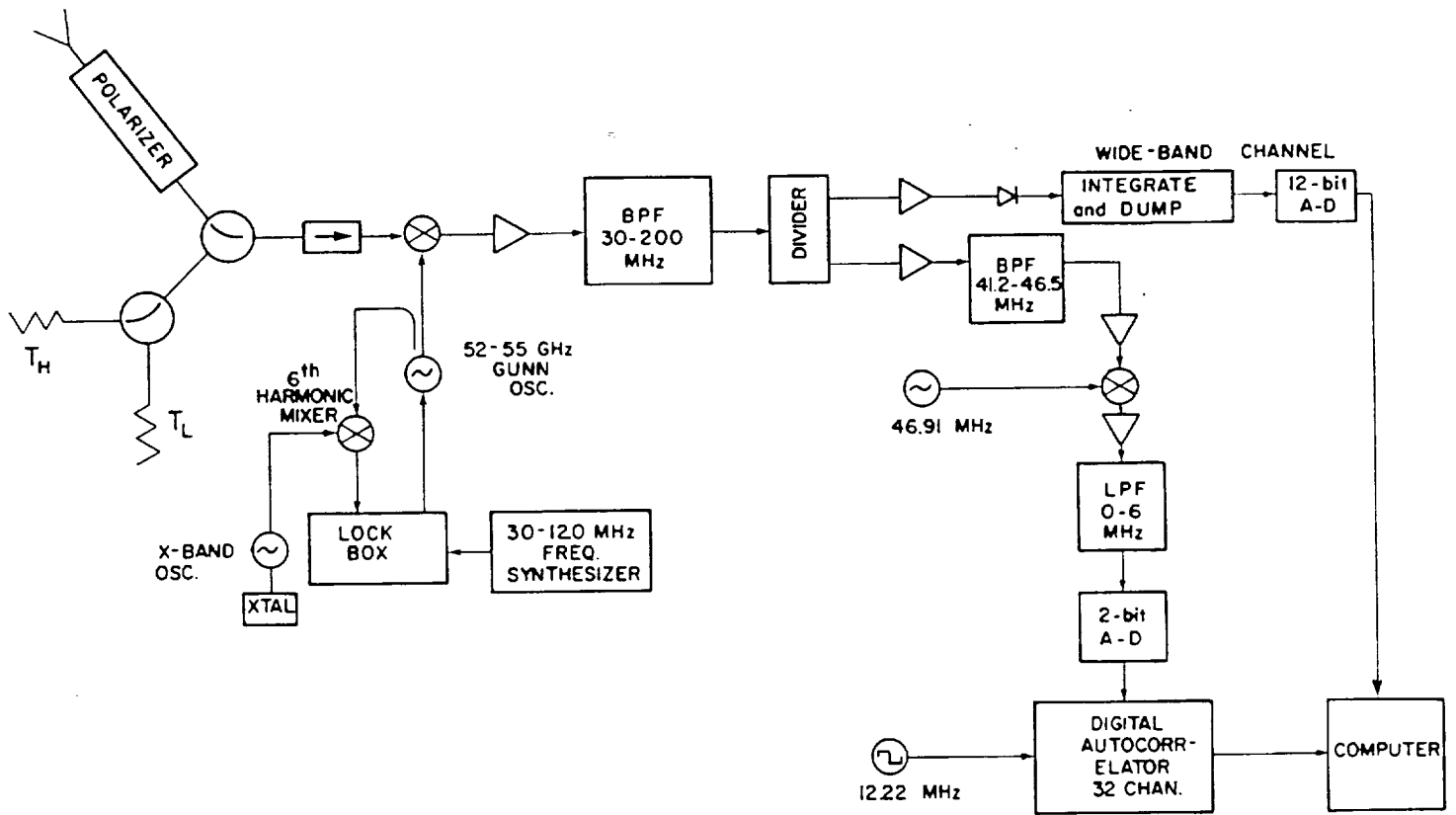Figure 5. Normalized contribution function for observation of the 27- oxygen line.

Figure 6. Proposed spectral-line system.

Figure 7. Illustration of the method of obtaining the water vapor burden u as a function of pressure P, given two estimated temperature profiles.

Figure 8. Predicted total temperature error energy versus forecast time, with measurement system resolution K_0 as a parameter.

Figure 9. Retrieved cell-top altitude versus altitude estimated by optical stereoscopy (Gasiewski and Staelin, 1989).

Figure 1. MTS instrument block diagram.

Figure 2. MTS weighting functions near 118 GHz.

Figure 3. Brightness temperatures observed near nadir by MTS on July 8, 1986, on a track over a series of convective cells (Gasiewski et al, 1990).

Figure 4. MTS brightness temperature perturbations (K) over Cyclone Oliver.

Figure 5. Normalized contribution function for observation of the 27- oxygen line.
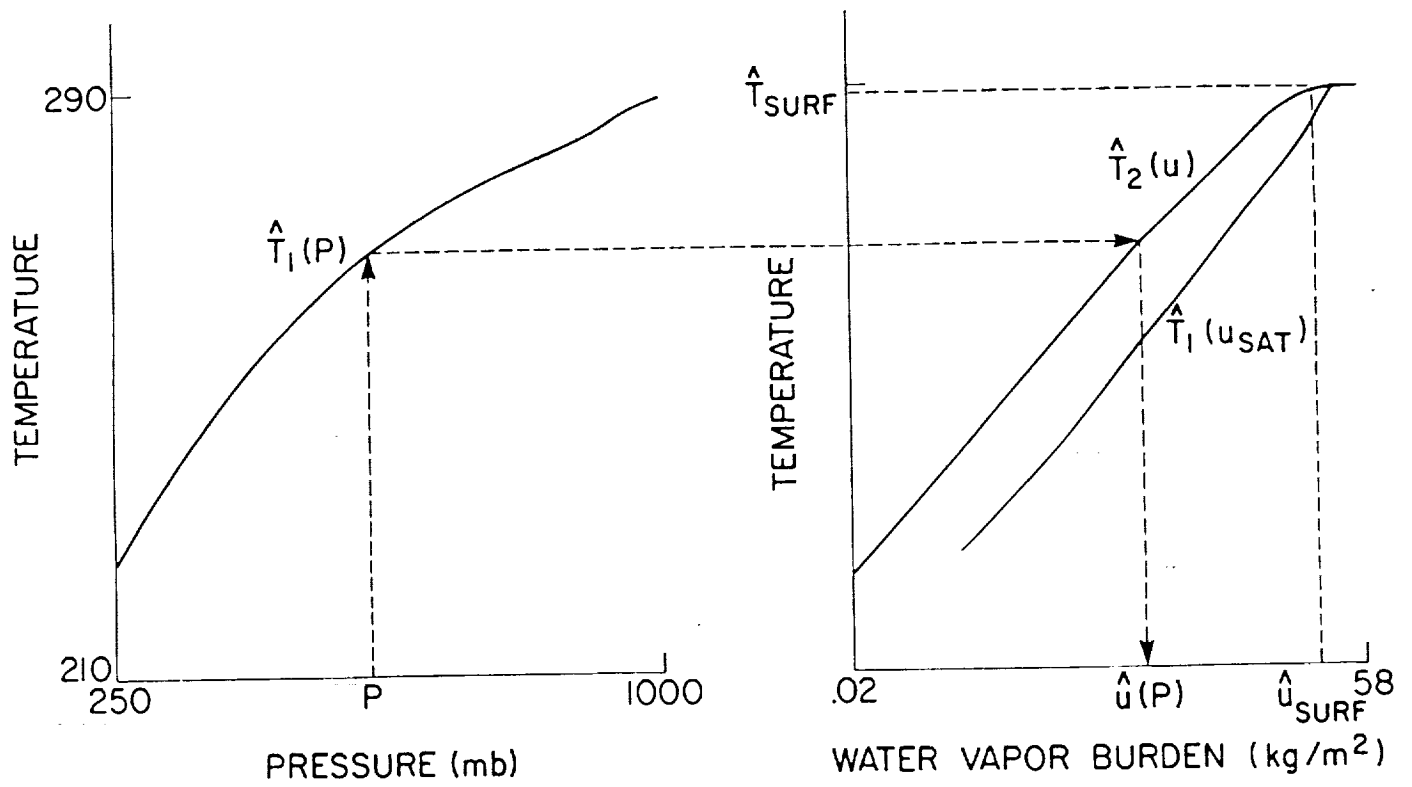
Figure 6. Proposed spectral-line system.

Figure 7. Illustration of the method of obtaining the water vapor burden u as a function of pressure P, given two estimated temperature profiles.
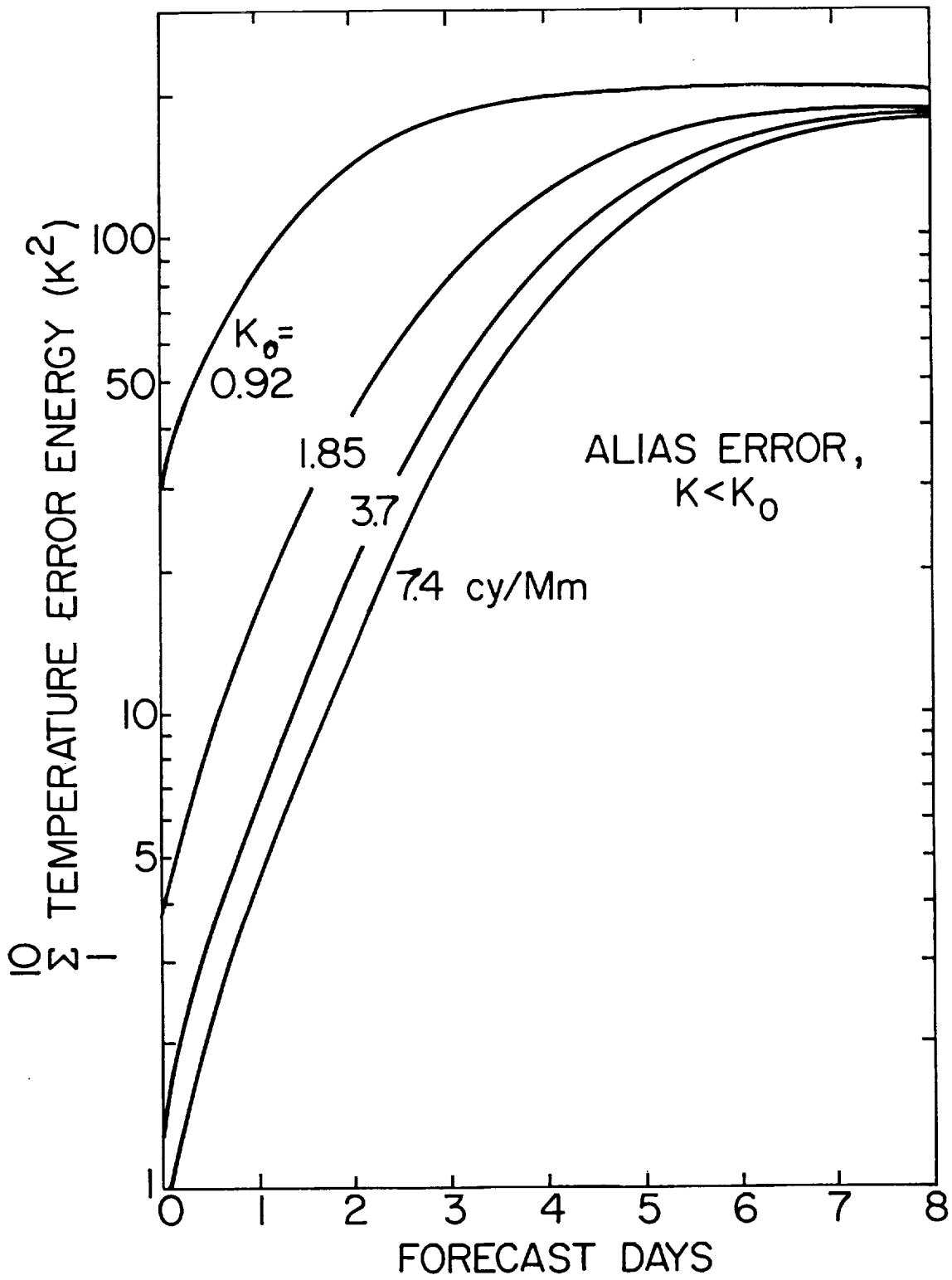
Figure 8. Predicted total temperature error energy versus forecast time, with measurement system resolution K_0 as a parameter.
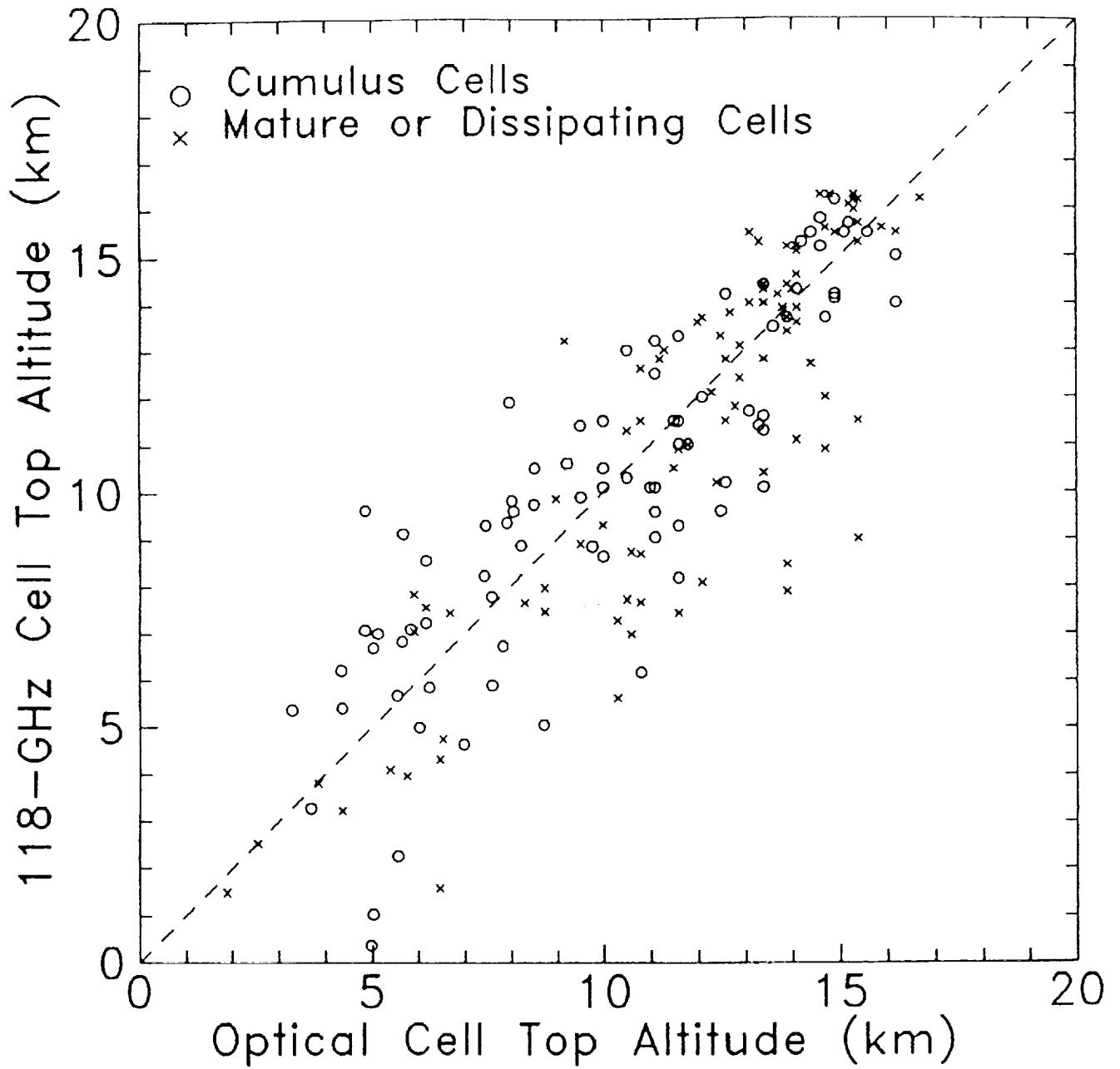
Figure 9.   Retrieved cell-top altitude versus altitude estimated by optical stereoscopy (Gasiewski and Staelin, 1989).